OPEN ACCESS

Original research

Disrupted spermatogenesis in a metabolic syndrome model: the role of vitamin A metabolism in the gut–testis axis

Teng Zhang,[1] Peng Sun,[1] Qi Geng,[1] Haitao Fan,[1] Yutian Gong,[1] Yanting Hu,[1] Liying Shan,[1] Yuanchao Sun,[2] Wei Shen,[3] Yang Zhou [1]

[1]State Key Laboratory of Reproductive Regulation & Breeding of Grassland Livestock, College of Life Sciences, Inner Mongolia University, Hohhot, China
[2]The Affiliated Hospital of Qingdao University and The Biomedical Sciences Institute of Qingdao University, Qingdao University, Qingdao, China
[3]College of Life Sciences, Qingdao Agricultural University, Qingdao, China

Correspondence to
Dr Yang Zhou, Inner Mongolia University, State Key Laboratory of Reproductive Regulation & Breeding of Grassland Livestock, Hohhot, China;
zhouyang106@126.com
Dr Teng Zhang;
zhangteng428@163.com

TZ and PS contributed equally.

Received 13 October 2020
Revised 11 January 2021
Accepted 11 January 2021

To cite: Zhang T, Sun P, Geng Q, *et al*. *Gut* Epub ahead of print: [*please include* Day Month Year]. doi:10.1136/gutjnl-2020-323347

ABSTRACT

Objective Effects of the diet-induced gut microbiota dysbiosis reach far beyond the gut. We aim to uncover the direct evidence involving the gut–testis axis in the aetiology of impaired spermatogenesis.

Design An excessive-energy diet-induced metabolic syndrome (MetS) sheep model was established. The testicular samples, host metabolomes and gut microbiome were analysed. Faecal microbiota transplantation (FMT) confirmed the linkage between gut microbiota and spermatogenesis.

Results We demonstrated that the number of arrested spermatogonia was markedly elevated by using 10× single-cell RNA-seq in the MetS model. Furthermore, through using metabolomics profiling and 16S rDNA-seq, we discovered that the absorption of vitamin A in the gut was abolished due to a notable reduction of bile acid levels, which was significantly associated with reduced abundance of *Ruminococcaceae_NK4A214_group*. Notably, the abnormal metabolic effects of vitamin A were transferable to the testicular cells through the circulating blood, which contributed to abnormal spermatogenesis, as confirmed by FMT.

Conclusion These findings define a starting point for linking the testicular function and regulation of gut microbiota via host metabolomes and will be of potential value for the treatment of male infertility in MetS.

Significance of this study

What is already known on this subject?
- Increasing evidence is showing that an excessive-energy diet-induced obesity is one of the risk factors for metabolic syndrome (MetS).
- Gut microbiota plays a pivotal role in metabolic disorders.
- Recent studies show that gut microbiota can have an impact on spermatogenesis.

What are the new findings?
- A MetS model induced by diets with excessive-energy levels resulted in a notable elevation in the number of abnormal testicular tubules and a sharp decline in spermatogonia differentiation.
- The vitamin A absorption was disrupted, which mainly due to the dramatically reduced abundance of bile acids induced by an imbalanced gut microbiota in the MetS model.
- The abnormal metabolic effects of vitamin A were transferable to the testicular cells through circulating blood, which contributed to the damaged spermatogenesis.
- The abnormal vitamin A metabolism contributed to damaged spermatogenesis in a gut microbiota dependent manner by using faecal microbiota transplantation.

How might it impact on clinical practice in the foreseeable future?
- These findings represent the beginning for linking the testicular function and regulation of gut microbiota via host metabolomes.
- Vitamin A metabolism might be applied to be a potential indicator for male infertility in individuals with MetS.
- The regulation of vitamin A metabolism through restoring the gut microbial ecosystem will be of value for male infertility therapy in individuals with MetS.

INTRODUCTION

Mounting evidence now suggests that excessive energy intake increases the risk factors for metabolic syndrome (MetS), which is seriously harmful to well-being and has become a major health issue worldwide; alarmingly, it is showing a younger trend, and its increasing prevalence is concomitant with the increased incidence of male infertility.[1]

Several studies demonstrate that the overconsumption of excessive energy alters male reproductive function and consequently impairs spermatogenesis.[2–6] Gut microbiota dysbiosis was observed in excessive energy diet-induced MetS.[7 8] Recently, Ding *et al*[9] showed that high-fat diet induced gut microbial dysbiosis with changeable phenotypes induced through faecal microbiome transplantation (FMT) leads to male infertility, confirming a causal relationship between the gut microbiota and spermatogenesis. In another study, Zhang *et al*[10] found that alginate oligosaccharide dosed mice showed an improvement in spermatogenesis following FMT, suggesting the possibility that FMT could potentially be used to treat patients in clinical research. These effects may be mediated through the metabolome, because the gut is ideally situated to sense an

excessive energy status and is capable of digestion and absorption of nutrients via the gut microbiota, further altering whole-body metabolism.[11 12] However, the way in which the gut–testis axis affects male infertility induced by MetS is largely unknown.

Herein, our findings elucidated the gut–testis axis mechanism responsible for damaging spermatogenesis in an induced excessive energy diet model. Furthermore, we uncovered the remodelling of the gut microbiota that resulted in reduced bile acid levels, which further influenced key intermediate vitamin A absorption. These findings demonstrated that modification of gut microbiota and alteration of vitamin A metabolism have potential as treatments for male infertility induced by MetS.

RESULTS

Metabolic disorders induced by diets with excessive energy levels resulted in impaired spermatogenesis

To study the influence of diets with excessive energy levels on spermatogenesis, we establish an excessive energy diet-fed sheep model (online supplemental tables 1 and 2). As expected, the medium-energy diet (MED) and high-energy diet (HED) groups had significantly increased body weight compared with the normal diet (ND) (standard chow diet) group (online supplemental figure 1A). The MED and HED groups also became glucose intolerant and developed insulin resistance, whereas the ND group did not (online supplemental figure 1B). Meanwhile, the HOMA-IR, QUICKI and Matsuda indexes were dramatically altered in the MED and HED groups (online supplemental figure 1C). Furthermore, fasting blood glucose and insulin concentrations were significantly increased in the HED group (online supplemental figure 1D). Serum low-density lipoprotein cholesterol and total cholesterol (TC) were largely increased in the MED and HED groups, while a significant reduction in high-density lipoprotein cholesterol was observed in the HED group (online supplemental figure 1E). These findings suggested that MetS sheep model was induced by diets containing excessive energy in the MED and HED groups.

Then, we investigated spermatogenesis by analysing H&E stained tissue samples and noted the presence of multinucleated giant cells and disorganised spermatogenic cells in the testes of the MED group (figure 1A). The impaired spermatogenesis became more severe in the HED group, where the number of spermatogenic cells was significantly reduced, and the spermatogenic epithelium became thinner (figure 1A). The percentage of histomorphologically abnormal tubules was significantly increased in the MED and HED groups compared with the ND group (figure 1B). Furthermore, H&E staining of cauda epididymis showed numerous mature sperm in ND group, but several cell debris was observed in the MED and HED groups (figure 1C). The epididymal spermatozoa concentration was lower in the MED and HED groups compared with that in the ND group (figure 1D). The spermatozoa morphology showed greater levels of abnormality in the MED and HED groups compared with the ND group (online supplemental figure 2). Cumulatively, our results suggest that MetS sheep model, induced by diets containing excessive energy, impaired spermatogenesis.

Deep analysis of 10× scRNA sequencing revealed that impaired spermatogenesis was due to the blocked differentiation of spermatogonia (SPG)

To define which spermatogenic cell subtypes were engaged in biological pathways or functions during impaired spermatogenesis in excessive energy diet-induced MetS sheep model, 10× Genomics analysis of testicular cells was performed (online supplemental figure 3A). The ratios of cell viability and aggregation are shown in online supplemental table 3.Filtered data were analysed together from the ND, MED and HED groups by using uniform manifold approximation and projection analysis to identify cell subtypes. Corresponding to known gene markers in different cell types in the testis, we identified nine clusters, including SPG, early spermatocytes (SPCs), late SPC, early round spermatids (Std), mid round Std, late round Std, Sertoli cells, Leydig cells and undefined cells (online supplemental figure 3B). The gene markers for nine clusters were shown in online supplemental figure 3C,D.

To elucidate the molecular nature of germ cell differentiation in impaired spermatogenesis induced by metabolic disorders, we calculated the percentage of each cell subtype, using only the germ cells from the ND, MED and HED group. As shown in figure 1E,F, significant difference was revealed in the SPG cluster (ND: 3.8%, MED: 6.58% and HED: 14.28%), early SPC cluster (ND: 7.86%, MED: 17.60% and HED: 22.99%) and late round Std cluster (ND: 41.00%, MED: 16.12% and HED: 14.36%) among the three treatment groups. Corresponding to the H&E staining results, spermatogenic cells were dramatically lower in the MED and HED groups, which indicated that SPG differentiation was disrupted. Hence, we set out to perform clustering analysis on SPGs (online supplemental figure 4A-E). This revealed four distinct cell clusters, which we defined as: (1) undifferentiated SPG (undiffed SPG), (2) differentiating SPG (diffing SPG), (3) differentiated SPG (diffed SPG), and (4) pre-leptotene SPC (pre-L-SPC), based on several gene markers as described previously.[13–15] To assess the developmental trajectory of these four SPG subsets, we performed monocle pseudotime trajectory analysis, which aligns individual cells along a developmental trajectory. It was revealed that these four SPG subsets had the following developmental order: undiffed SPG →diffing SPG →diffed SPG →pre-L-SPC (figure 1G,H). Meanwhile, the existence of branched point from the linear path of the pseudotime trajectory was observed, demonstrating that one branched group of cells represented the differentiation from undiffed SPG to diffed SPG and pre-L-SPC; the other branched group of cells represented the transition state that bridged the undiffed SPG and diffing SPG stages, which were likely to be SSC pool enriched, simultaneously generating progenitor SPG that initiated spermatogenic differentiation (figure 1I).

In order to explore the mechanism of SPG differentiation retardation in MetS sheep model, Gene Ontology (GO) analysis was performed to demonstrate that distinct categories of differentially expressed genes were enriched in the ND versus MED group and ND versus HED group (figure 1J). 'Reproductive process' and 'metabolic process' were highly enriched in GO terms of SPG clusters in ND versus MED and ND versus HED, which suggested that metabolic process was consistent with reproductive process and was significantly altered during SPG differentiation.

The absorption of vitamin A was disrupted due to a drastic reduction in levels of bile acids in the MetS model

To address whether the arrest of SPG differentiation was closely connected with gut metabolism, we examined the untargeted metabolome profiles generated on intestinal digesta samples using ultra-high performance liquid chromatography-quadrupole time-of-flight mass spectrometry. Using partial least squares discriminant analysis, we observed distinct clustering of metabolites among the ND, MED and HED groups (figure 2A and online supplemental figure 5A). The excessive energy diet was

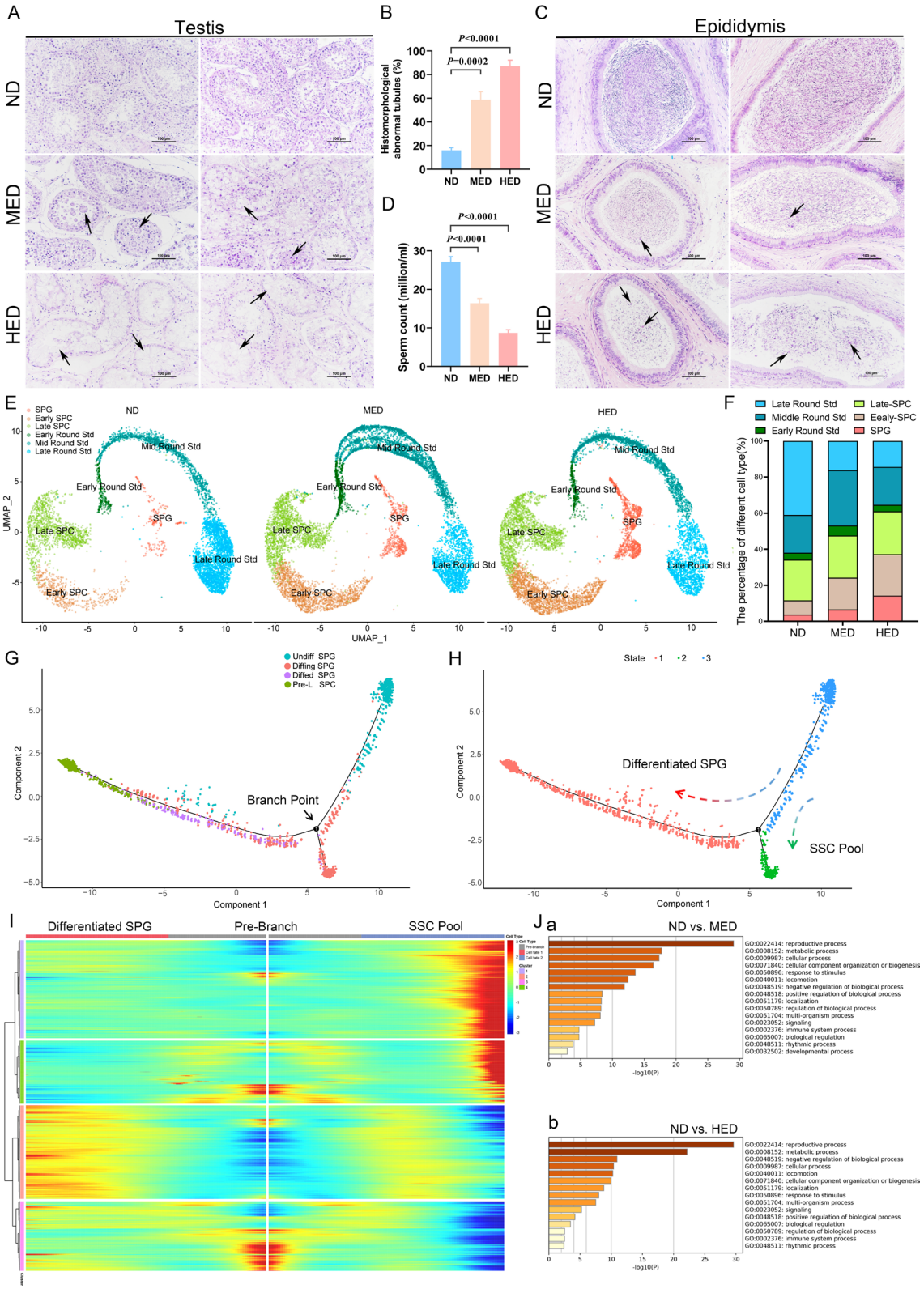

Figure 1 High-caloric load induced by excessive energy intake disrupted spermatogenesis in a metabolic syndrome (MetS) model. (A) The representative testicular sections are stained with H&E. Scale bar=100 µm. (B) The percentage of abnormal tubules in testicular samples from each group (n=5). (C) The representative epididymal sections are stained with H&E. (D) Statistical analysis of sperm counts (n=5). (E) UMAP plot of germ cell clusters in testes defined by scRNA-seq analysis. (F) The percentage of each germ cell cluster from three groups. (G) Single-cell trajectories of SPG subsets are shown with cells ordered in pseudotime. Branch point represents distinct germ cell transition states. (H) The SPG trajectory is colored by three cell states. (I) Heatmap represents significant DEGs between each cluster at differentiated SPG and SSC pool stages at branch point. (J) Gene Ontology terms of differentially expressed genes (DEGs) in the SPG cluster from (a) ND versus MED and (b) ND versus HED groups. HED, high-energy diet; MED, medium-energy diet; ND, normal diet; scRNA-seq, single-cell RNA-seq; SPC, spermatocytes; SPG, spermatogonia; SSC, spermatogonia stem cell; UMAP, uniform manifold approximation and projection.

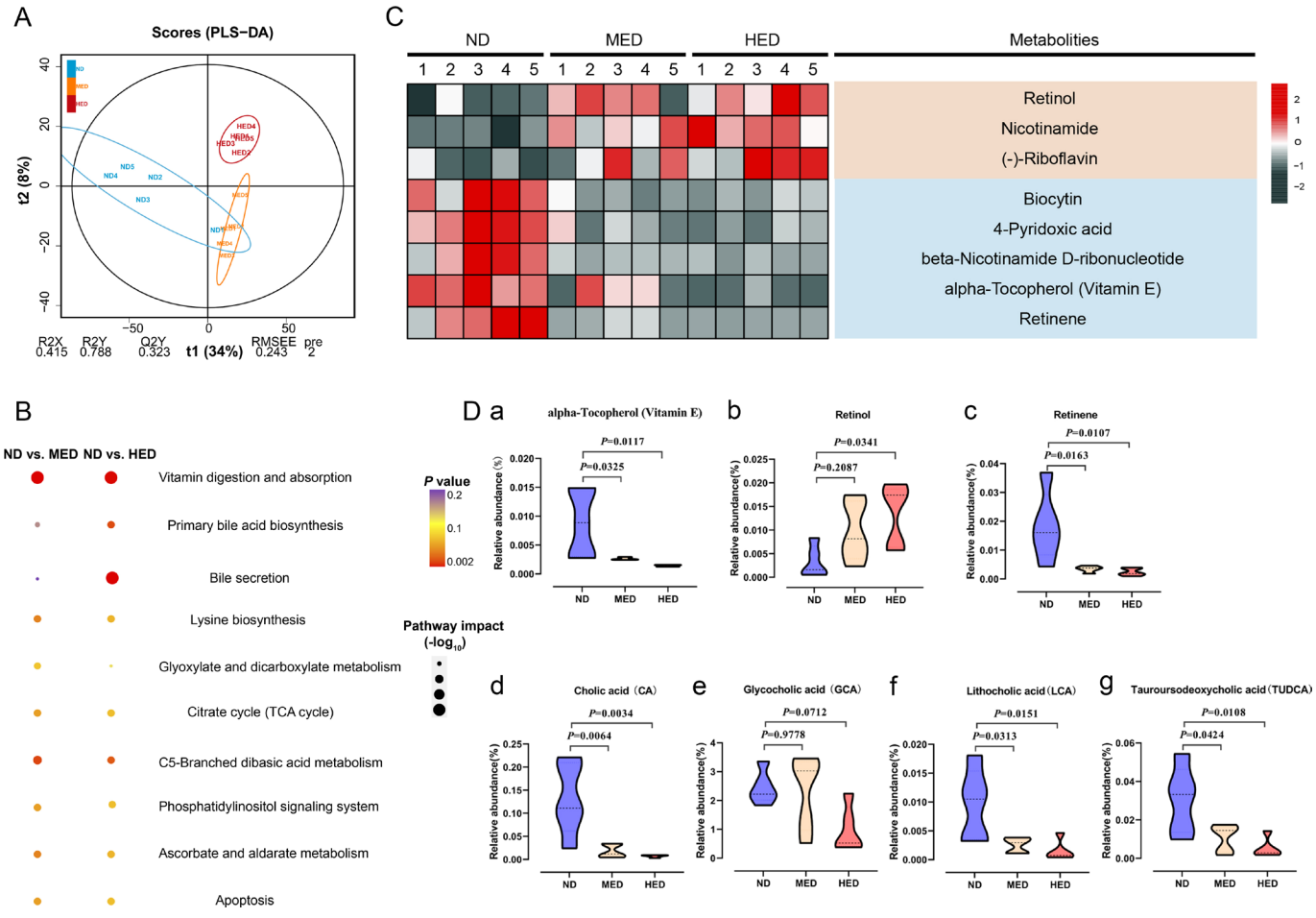

Figure 2 Absorption of vitamin A was disturbed in a MetS model. (A) Orthogonal projections to latent structures-discriminant analysis (PLS-DA) score plot for discriminating the intestine digesta metabolome from the ND, MED and HED groups (n=5). (B) Disturbed metabolic pathways in the ND versus MED and ND versus HED groups. (C) Heatmaps of the differential metabolites including eight vitamins that were altered through MED and HED feeding compared with ND feeding. (D) Comparison of the relative abundance of (a) vitamin E, (b) retinol, (c) retinene, (d) cholic acid, (e) glycocholic acid, (f) lithocholic acid and (g) tauroursodeoxycholic acid in the indicated groups. HED, high-energy diet; MED, medium-energy diet.

sufficient to trigger widespread changes in metabolites (online supplemental figure 5B, C). Interestingly, these two comparisons had 250 common differential metabolites altered, and they were mainly enriched in the vitamin digestion and absorption KEGG pathway (figure 2B). The differential metabolites enriched in the vitamin digestion and absorption pathway were comprised of three fat-soluble vitamins and five water-soluble vitamins (figure 2C). Owing to the bile acid associated pathway also being enriched, we hypothesised that the absorption of fat-soluble vitamins was affected by bile acid levels. There are three fat-soluble vitamins: retinol, retinene and alpha-Tocopherol (vitamin E). Retinol and retinene are the bioactive forms of vitamin A, and they can be transformed into each other in vivo and have the same function. Retinene may be further oxidised to retinic acid, but this is an irreversible process. Vitamin E is an antioxidant that promotes vitamin A absorption. We found that the relative abundance of vitamin E was decreased in the MED and HED groups compared with the ND group (figure 2Da), thus influencing vitamin A absorption in the former groups. Notably, the relative abundance of retinol was dramatically increased, while the relative abundance of retinene was dramatically decreased in the MED and HED groups compared with that in the ND group (figure 2Db,Dc). In order to define the differences of the metabolites were not from the discrepancy in different diets, the measurement of retinol and retinene levels was performed and showed no significant difference among the ND, MED and HED groups (online supplemental figure 6). These results suggested that vitamin A absorption was disturbed in the MetS model. The abundance of retinol was increased, whereas the abundance of retinene was decreased; this was because little retinol was transformed into retinene, and retinol was lost instead of being absorbed. Additionally, the relative abundance of glycocholic acid was not altered, whereas the relative abundances of cholic acid (CA), lithocholic acid (LCA) and tauroursodeoxycholic acid (TUDCA) were dramatically decreased (figure 2Dd-g). Taken together, these untargeted metabolome profiles demonstrated that the absorption of vitamin A was dysregulated by reduced bile acid levels in the MetS model.

Gut microbiota dysbiosis was induced in the MetS model

The gut microbiota plays a vital role in its hosts metabolism by interacting with the host's signalling pathways[16 17]; therefore, we examined bacterial 16S rDNA sequencing of intestinal digesta. Rarefaction curve examination revealed that the data were reliable for further analysis (online supplemental figure 7A). A distinct clustering of microbiota composition for the three treatment groups was observed using Bray-Curtis based

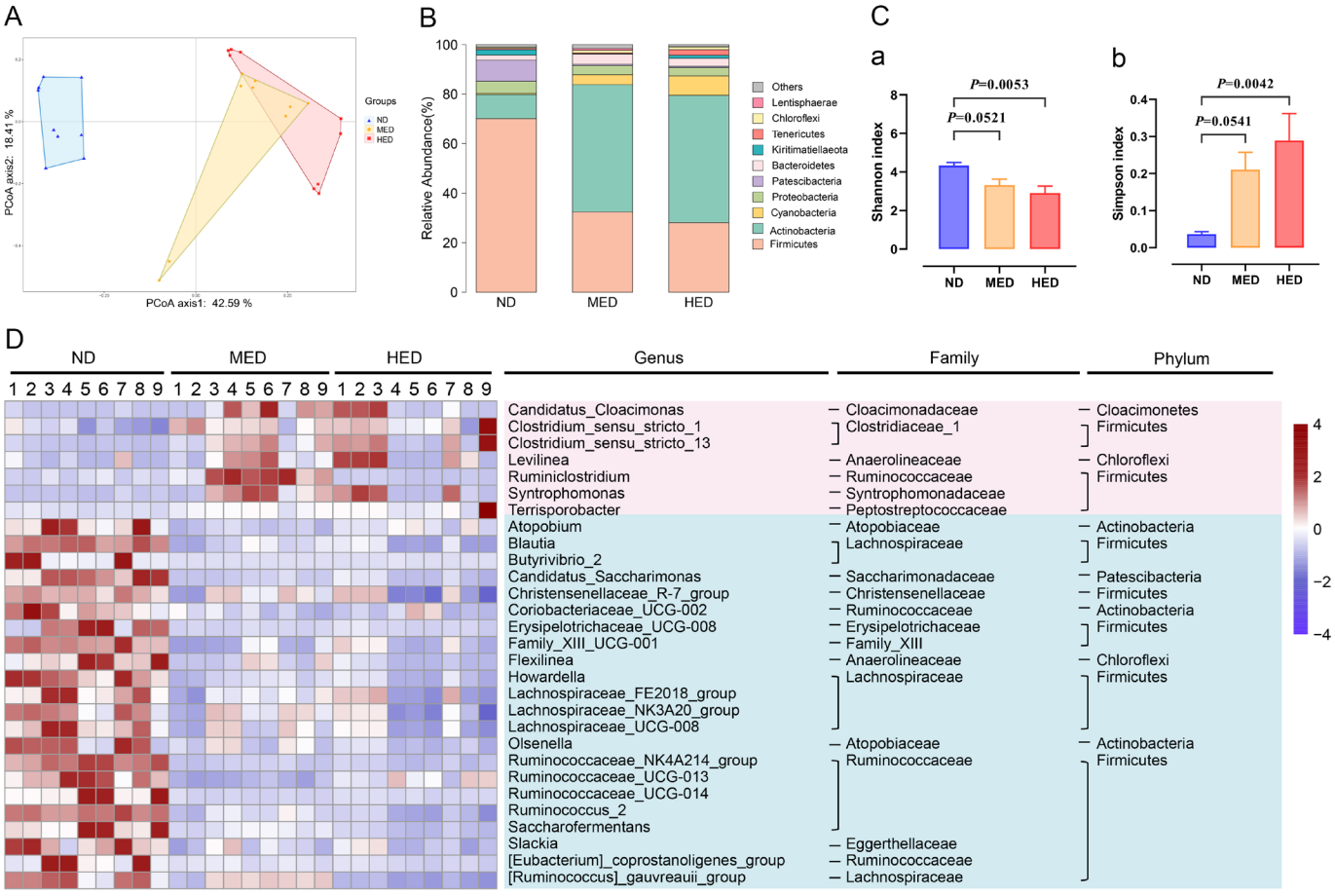

Figure 3 Profiling of the gut microbiota was altered in a MetS model. (A) Bray-Curtis principal coordinate analysis (PCoA) plot of gut microbiota based on the operational taxonomic unit metrics of the samples in the ND, MED and HED groups (n=9). (B) Bacterial taxonomic profiling at the phylum level of intestinal bacteria from different treated groups. (C) (a) Shannon index and (b) Simpson index of gut microbiota in three treated groups. (D) Heatmap of differential abundance from the MED and HED groups compared with the ND group. The color of the spots in the left panel represents the relative abundance at the genus level in each group. HED, high-energy diet; MED, medium-energy diet; MetS, metabolic syndrome.

principal coordinates analysis (figure 3A). To assess the overall composition of the bacterial community in different groups, the degree of bacterial taxonomic similarity of gut microbiota was analysed at the phylum level (figure 3B). Moreover, Shannon curves, OTU rank curves, Shannon index and Simpson index of gut microbiota were significantly altered, indicating that the richness and diversity of the gut microbiota was reduced in the MED and HED groups (figure 3C and online supplemental figure 7A). Furthermore, the twenty-nine bacteria altered at the genus level in the MED and HED groups compared with the ND group (figure 3D). Genus-level analysis showed that most of these altered bacteria belonging to *Firmicutes*, *Ruminococcaceae* and among these genus-level bacteria, the relative abundances of *Ruminococcus_2* and *Ruminococcaceae_NK4A214_group* were significantly decreased in the MED and HED groups compared with ND in an energy dose-dependent manner after the long-term high-calorie challenge (online supplemental figure 7B).

The physiological function of bile acids includes the promotion of absorption of fat-soluble vitamin A. It is revealed that CA, LCA and TUDCA were related with retinol, and they were also correlated with retinene by using pearson's correlation analysis (figure 4 and online supplemental figure 8A). To investigate the functional relationship between gut microbial dysbiosis and bile acid levels, Spearman's correlation analysis was performed. As shown in figure 4B, Spearman's correlation analysis between CA, LCA TUDCA and differential genus-level bacteria revealed that the numbered bacteria 4, 9, 15, 17, 19, 21 and 27 were significantly correlated with CA, LCA and TUDCA. Combined with the relative abundance of these bacteria (online supplemental figures 7B and 8B), *Ruminococcaceae_NK4A214_group* showed a strong correlation with CA, LCA and TUDCA (figure 4C). Cumulatively, *Ruminococcaceae_NK4A214_group* was dramatically downregulated, which in turn had a profound influence on bile acid levels and further affected host vitamin A absorption in the MetS model.

Vitamin A metabolism dysfunction was transferable to host testes in the MetS model

In order to deeply investigate the mechanism of impaired spermatogenesis, we verified vitamin A metabolism in the testis. First, we performed targeted metabolomics profiling of the vitamin A level in testis samples from different treated groups using liquid chromatography–MS. Vitamin A levels were significantly decreased in the HED group compared with the ND group (figure 5A). Furthermore, we detected the vitamin A level in serum using an ELISA kit and found that the data pointed towards a similar trend as that in the testis (figure 5B). Testicular cells receive vitamin A from the blood, and blood serum vitamin A is bound by retinol binding protein 4 (RBP4). Vitamin

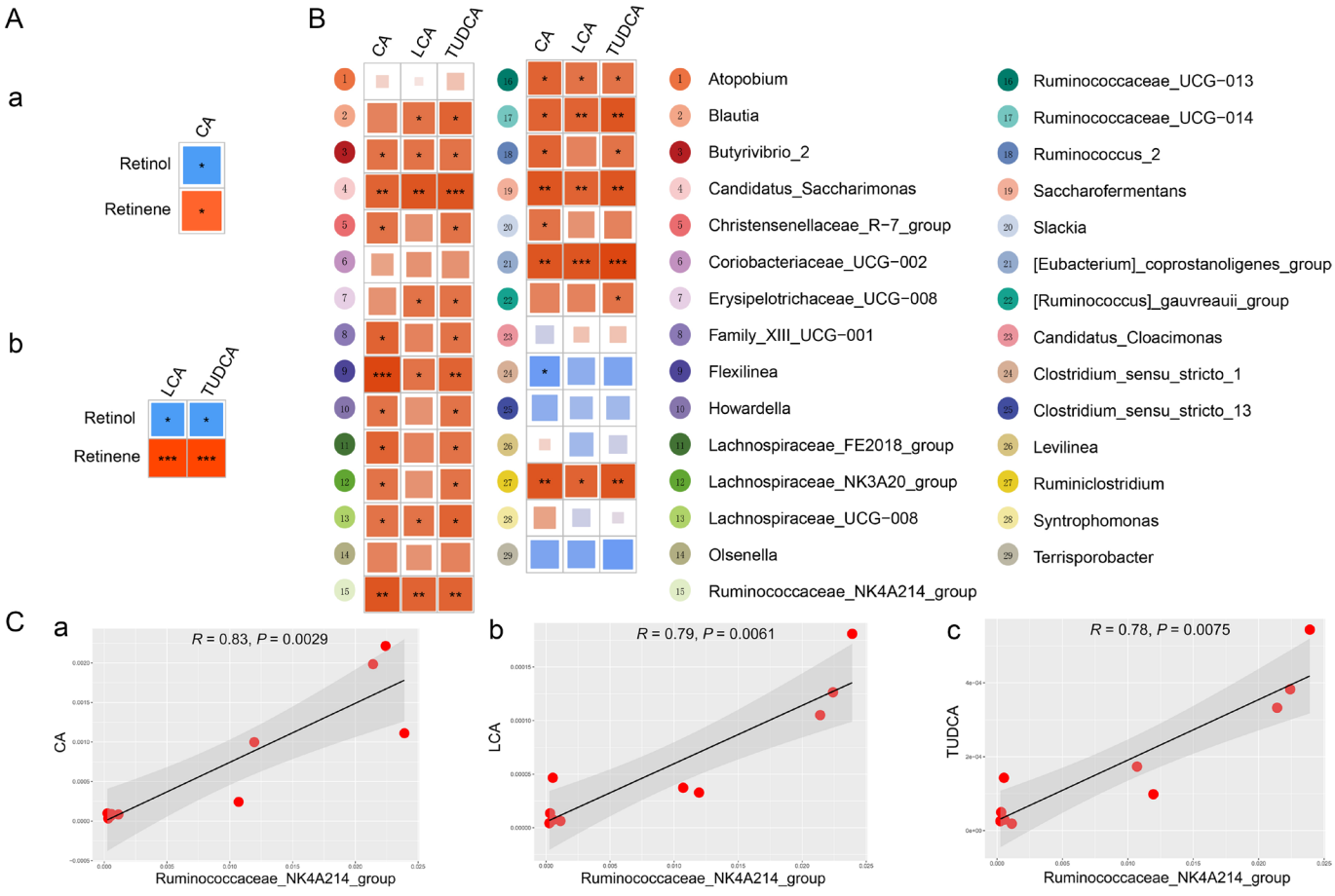

Figure 4 The alteration of gut microbiota was closely associated with the bile acid levels. (A) Pearson's correlations of retinol and retinene levels with the levels of (a) CA, (b) LCA and TUDCA. Red indicates a positive correlation, and blue indicates a negative correlation. (B) Spearman's correlation analysis of differential genus microbiota levels with CA, LCA and TUDCA levels. (C) Spearman's correlation analysis of Ruminococcaceae_NK4A214_group abundance with (a) CA, (b) LCA and (c) TUDCA levels. CA, cholic acid; LCA, lithocholic acid; TUDCA, tauroursodeoxycholic acid.

A can also be transported into testicular cells via RBP4 delivery to membranes. Therefore, we examined the expression levels of RBP4 using immunofluorescent (IF) staining and western blot. Results showed that the expression level of RBP4 was significantly decreased in the MED and HED groups compared with that in the ND group (figure 5C). These results corresponded to the vitamin A level tests in the LS-MS and ELISA experiments.

The 10× scRNA-seq results given previously indicated that differentiation from undiffed SPG to pre-L-SPC was partly blocked. PLZF is expressed in SPG, which is a marker gene of undifferentiated SPG for maintaining self-renewal of SSCs.[18] As shown in online supplemental figure 9, the expression level of PLZF was upregulated in the testis by using IF staining and western blot in the MED and HED groups compared with the ND group. In addition, the expression of marker genes of meiosis in pre-L-SPC are detected, and we found that STRA8 and SYCP3 expression levels displayed a sharp decrease, as shown by IF staining (figure 5D) and western blot (figure 5E,F).

In the present study, the damage during spermatogenesis resulted from the downregulated expression of meiotic gene markers, and vitamin A metabolism played a vital role in meiotic gene activation. To further assess whether RDH10 levels were changed in the testis, we identified the expression level of RDH10 using IF staining and western blot and found that it was downregulated in the MED and HED groups compared with the ND group (figure 5C, E,F). Together, these results suggested that vitamin A metabolism was abnormal, thus the reduced levels of vitamin A and RDH10 contributed to the compromised impaired spermatogenesis in testes in the MetS model.

Perturbative vitamin A metabolism led to impaired spermatogenesis in a gut microbiota dependent manner

To investigate the effect of the gut microbiota on impaired spermatogenesis phenotypes in the MetS model, microbiota of the intestinal digesta taken from the ND and HED groups was transplanted into mice by oral gavage (figure 6A). After 8 weeks of colonisation, the body weight (online supplemental figure 10A), serum TC levels (online supplemental figure 10B) and serum TG levels (online supplemental figure 10C) did not show any significant difference between ND-FMT (mice transplanted with microbiota from the ND controls) and HED-FMT (mice received the HED microbiota). However, HED-FMT displayed a significant decrease in testicular vitamin A levels, compared with those mice in the ND-FMT (figure 6B). To further confirm that the differential testis vitamin A levels in the FMT groups were due to the alteration of the colonised gut microbes instead of the vitamin A and bile acids levels transmitted from the donors, we examined the transmitted material from the donors ND and HED groups. The transplanted material was prepared by strict dilute and homogenise filter procedure, and we found that the levels of retinol, retinene and bile acids had no significant difference in the two donor groups (online supplemental figure 11A-C). In addition, we detected the abundance of the

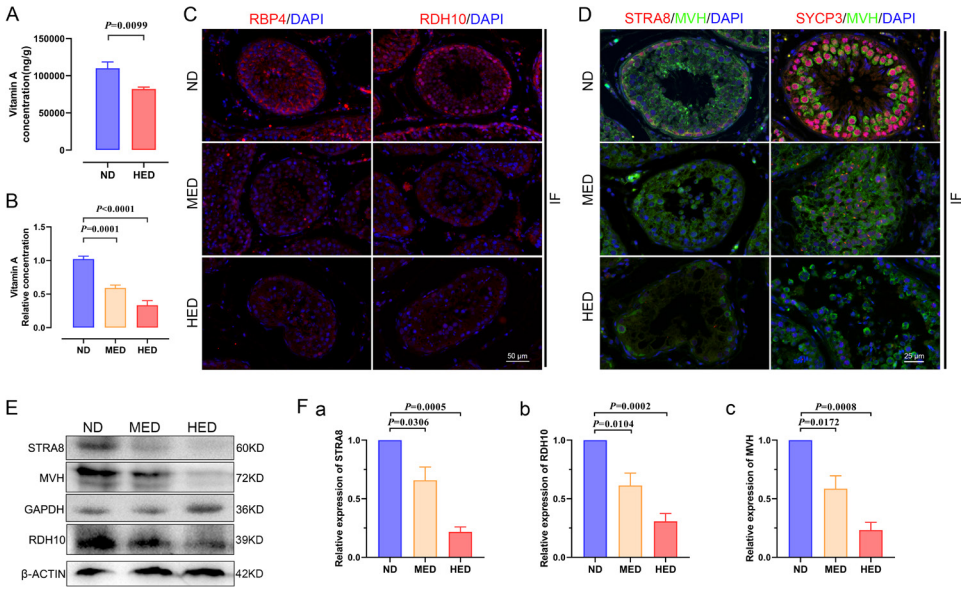

Figure 5 The effect of abnormal vitamin A metabolism was transferable to testis. (A) The testicular vitamin A levels of the ND and HED fed groups were measured (n=6). (B) Serum vitamin A levels of the ND, MED and HED-fed groups were examined (n=6). (C) The representative images of RBP4 and RDH10 immunofluorescent (IF) staining in sections of testicular tissue. Scale bar=50 µm. (D) The IF staining for STRA8 and SYCP3 is shown together with MVH in representative sections of testicular tissue. Scale bar=25 µm. (E) Western blot of STRA8, RDH10, MVH, GAPDH and β-ACTIN in each indicated group. (F) Quantification protein levels of (a) STRA8, (b) RDH10 and (c) MVH. HED, high-energy diet; MED, medium-energy diet.

Ruminococcaceae_NK4A214_group in the transmitted material from the donors and found that the abundance of the *Ruminococcaceae_NK4A214_group* was dramatically decreased in the HED group compared with that in the ND group (online supplemental figure 12A). We also analyse the abundance of the *Ruminococcaceae_NK4A214_group* in the ND-FMT and HED-FMT by PCR and qPCR and found that the abundance of *Ruminococcaceae_NK4A214_group* was significantly decreased in the HED-FMT group compared with ND group (figure 6C and online supplemental figure 12B).

To confirm that microbiota transplantation modulated spermatogenesis, we conducted H&E staining to examine testicular morphology. This revealed that testicular tissue from mice transplanted with ND microbiota exhibited normal testicular development, whereas tissue from mice transplanted with microbiota from the HED group exhibited thinning of the seminiferous epithelium and detachment of testicular cells from the basement membrane of the seminiferous tubules; in addition, some spermatogenic cells were dead and shed into the luminae of the tubules (figure 6D). The percentage of abnormal tubules was observed between the ND-FMT and HED-FMT; ND-FMT had approximately 12% abnormal tubules, while HED-FMT had more than 47% (figure 6E). The expression levels of STRA8 and RDH10 were determined by IF staining (figure 6F) and western blot (figure 6G,H), and HED-FMT had dramatically decreased protein expression, which was similar to the results of the MetS model. Collectively, these results demonstrated that the recipient mice recapitulated microbial and metabolic phenotypes as observed in the metabolic disorder model, and gut microbiota mediated the disturbed metabolism of vitamin A, which led to damaged spermatogenesis.

DISCUSSION

MetS has become a major health issue worldwide. Male infertility in MetS is commonly accompanied by gut microbiota dysbiosis. However, there are only a limited selection of therapeutic treatments for male infertility patients with MetS. Therefore, the gut–testis axis in the aetiology of male infertility in MetS is worthy of exploration. First, we conducted a detailed phenotypic assessment of impaired spermatogenesis from a MetS model induced by an excessive energy diet and revealed a notable elevation in the number of abnormal tubules and a sharp decline in SPG differentiation. Furthermore, disruption of vitamin A absorption in the intestine was observed in the MetS model. Notably, the absorption of fat-soluble vitamins was affected by reduced bile acid levels and was strongly correlated with the abundance of *Ruminococcaceae_NK4A214_group* in the MetS model. These findings suggested that disruption of the absorption of vitamin A was mainly due to the dramatically reduced abundance of these bile acids induced by an imbalance in the homeostasis of gut microbiota. Lastly, the pivotal role of vitamin A metabolism in the gut–testis axis was uncovered in our study. This finding indicated that, through its ability to restore the gut microbial ecosystem, vitamin A metabolism might be a potential candidate for the treatment of male infertility in individuals with MetS (figure 7).

Adequate vitamin A is essential for male and female reproduction as well as embryonic development.[19 20] Vitamin A is particularly important for its role in the process of meiotic initiation in the female gonad during embryogenesis and in the male gonad postnatally. Vitamin A is the molecular precursor of retinoic acid (RA), and RA is indispensible for meiotic initiation and also activates the gatekeeper gene of meiosis *STRA8*.[21–27] RA is metabolised from retinol by two successive oxidation reactions. In the first step, retinol is reversibly converted to retinaldehyde (RAL) mainly by the enzyme RDH10.[28 29] In the second step, RAL can then be oxidised to form RA mediated by members of the aldehyde dehydrogenase 1A family.[30] Several studies report that vitamin A deficient rodents suffer male infertility mainly owing to a deficiency of RA.[31] In the clinical research, it is indicated that germ cell aplasia is associated with local deregulation of vitamin A metabolism.[32] Recently, evidence has demonstrated

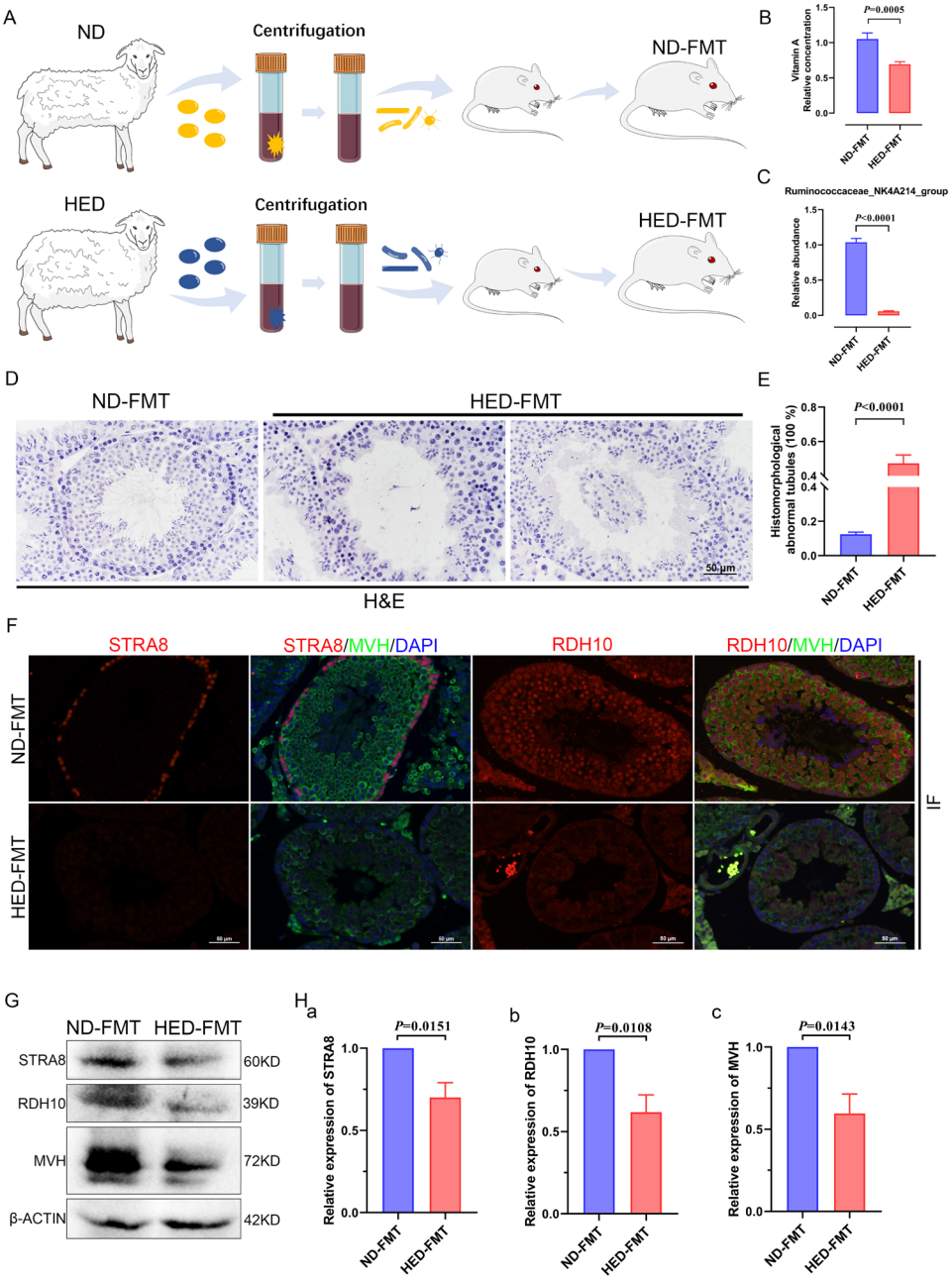

Figure 6 Faecal transplants of HED microbiota exhibited disrupted spermatogenesis induced by a notable reduction in levels of vitamin A and RDH10. (A) Study design diagram of the faecal transplant experiment. (B) Vitamin A level measured using an ELISA kit (n=6 for ND-FMT; n=10 HED-FMT). (C) The qPCR analysis of Ruminococcaceae_NK4A214_group abundance (n=9). (D) H&E staining of ND-FMT and HED-FMT testicular tissue. (E) Percentage of abnormal tubules in testicular tissue from each group (n=7). (F) Representative IF staining images of STRA8 and RDH10 in sections of testicular tissue. Scale bar=50 μm. (G) Western blotting of STRA8, RDH10, MVH and β-ACTIN in each indicated group. (H) Quantification protein levels of (a) STRA8, (b) RDH10 and (c) MVH. FMT, faecal microbiome transplantation; HED, high-energy diet; IF, immunofluorescent.

on the relationship between vitamin A status and MetS.[33–36] Furthermore, some reports suggested that vitamin A deficiency is a possible independent risk factor for MetS.[37 38] However, whether an association between MetS and infertility in the vitamin A deficiency has not been uncovered. Organisms work as a whole, so an interference in one organ is likely to impact the body's homeostatic balance and lead to damage in other related organs. To the best of our knowledge, the current findings are the first to show that the abnormal vitamin A metabolic process was strongly mediated by bile acid dysregulation and gut microbiota dysbiosis, resulting in the impairment of male fertility via circulating blood in the MetS model. Additionally, the expression of RDH10, an enzyme that is essential in the conversion of retinol to RAL, exhibited a sharp reduction, which was mainly due to feedback following the decreased abundance of vitamin A in the testis.

The gut microbiota is regarded as a metabolic organ that regulates its hosts metabolism. Meanwhile, the abundance of bile acids as a signalling molecule in metabolically active tissues such as the gut has aroused great interest in metabolic disorders. Furthermore, it is known that the interaction between the gut microbiome and bile acids is not unidirectional. On the one hand, the gut microbiota can regulate the size of the bile acid pool and the ratio of bile acid composition. On the other hand,

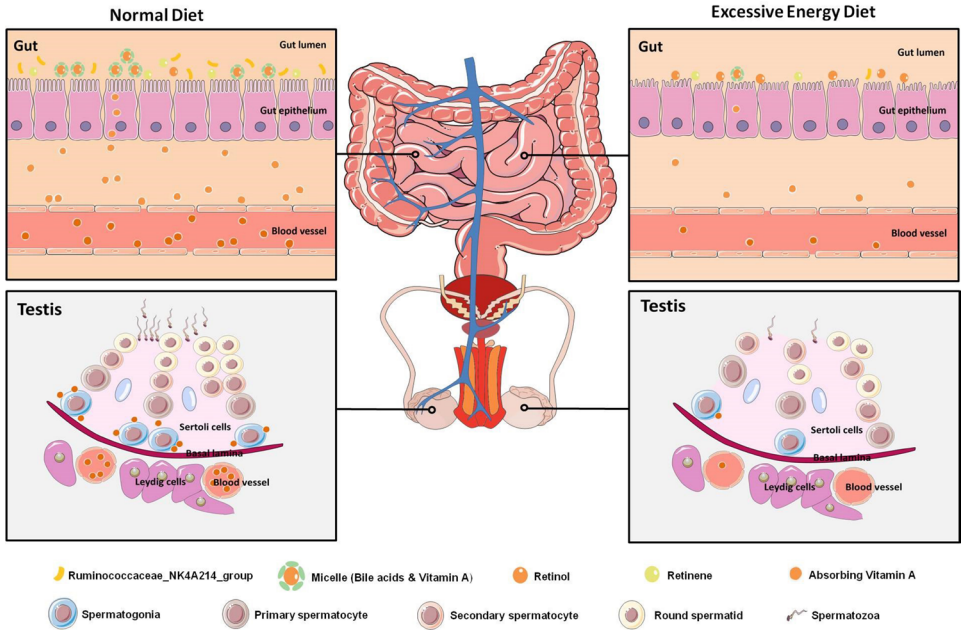

Figure 7 Graphical abstract. Diagram illustrating the proposed vitamin A metabolism via the gut–testis axis being indispensable for spermatogenesis. The disrupted vitamin A absorption was affected by reduced bile acid levels, which mainly due to the dramatically decreased abundance of Ruminococcaceae_NK4A214_group. Notably, the abnormal vitamin A metabolism were transferable to the testicular cells through the blood circulation, which led to abnormal spermatogenesis in the MetS model. MetS, metabolic syndrome.

bile acid is one of the main components of bile; a healthy concentration is necessary for the dissolution, digestion and absorption of lipids and fat-soluble vitamins from food. In the present study, using KEGG pathway analysis, we found that the common differential metabolites in intestinal digesta from the MED and HED groups, when compared with the ND group, were also mainly enriched in the bile acid related pathway, which indicated that bile acids have an influence on vitamin A absorption. Additionally, correlation analyses of bile acid levels and genus-level bacteria revealed that CA, LCA and TUDCA were correlated strongly with *Ruminococcaceae_NK4A214_group*. Our findings suggest that the modulation of gut microbiota altered bile acids levels and further affected vitamin A absorbtion in the host gut, and the abnormal vitamin A metabolism was transferable to the testis through the blood circulation, resulting in damaged spermatogenesis in the MetS model. We therefore suggest that this study may have promising therapeutic value for male infertility induced by MetS.

Acknowledgements We would like to thank Fei Gao for critical reading of this manuscript and contribution to the discussions. We would also like to thank Fiona Stansfield for critical reading of this manuscript.

Contributors YZ designed and supervised the study; TZ, PS, QG, HF, YG, YH, LS and YS performed the experiments and analysed the data; YZ and TZ wrote the manuscript; YZ, TZ and WS contributed to the manuscript revision and discussion. All the authors read the manuscript and approved the final manuscript.

Funding This study was supported by the National Natural Science Foundation of China (31900595 to YZ; 32000582 to TZ), the opening project of the State Key Laboratory of R^2BGL (SKL-IT-201810 to YZ; SKL-OT-201903 to TZ).

Competing interests None declared.

Patient consent for publication Not required.

Ethics approval All animal procedures were approved and conducted in accordance with the Inner Mongolia University Animal Care and Use Committee.

Provenance and peer review Not commissioned; externally peer reviewed.

Data availability statement All data relevant to the study are included in the article or uploaded as supplementary information. Data are available on reasonable request. Data sets generated and analysed during this study are available from the corresponding author on reasonable request.

ORCID iD

Yang Zhou http://orcid.org/0000-0003-1768-0244

REFERENCES

1 Rato L, Alves MG, Cavaco JE, *et al*. High-Energy diets: a threat for male fertility? *Obes Rev* 2014;15:996–1007.
2 Attaman JA, Toth TL, Furtado J, *et al*. Dietary fat and semen quality among men attending a fertility clinic. *Hum Reprod* 2012;27:1466–74.
3 Jensen TK, Heitmann BL, Blomberg Jensen M, *et al*. High dietary intake of saturated fat is associated with reduced semen quality among 701 young Danish men from the general population. *Am J Clin Nutr* 2013;97:411–8.
4 Hammoud AO, Wilde N, Gibson M, *et al*. Male obesity and alteration in sperm parameters. *Fertil Steril* 2008;90:2222–5.
5 Crean AJ, Senior AM. High-Fat diets reduce male reproductive success in animal models: a systematic review and meta-analysis. *Obes Rev* 2019;20:921–33.
6 Deshpande SS, Nemani H, Pothani S, *et al*. Genetically inherited obesity and high-fat diet-induced obesity differentially alter spermatogenesis in adult male rats. *Endocrinology* 2019;160:220–34.
7 Zeng S-L, Li S-Z, Xiao P-T, *et al*. Citrus polymethoxyflavones attenuate metabolic syndrome by regulating gut microbiome and amino acid metabolism. *Sci Adv* 2020;6:eaax6208.
8 Fan Y, Pedersen O. Gut microbiota in human metabolic health and disease. *Nat Rev Microbiol* 2021;19:55–71.

9 Ding N, Zhang X, Zhang XD, *et al*. Impairment of spermatogenesis and sperm motility by the high-fat diet-induced dysbiosis of gut microbes. *Gut* 2020;69:1608–19.
10 Zhang P, Feng Y, Li L, *et al*. Improvement in sperm quality and spermatogenesis following faecal microbiota transplantation from alginate oligosaccharide dosed mice. *Gut* 2021;70:222–5.
11 Turnbaugh PJ, Ley RE, Mahowald MA, *et al*. An obesity-associated gut microbiome with increased capacity for energy harvest. *Nature* 2006;444:1027–31.
12 David LA, Maurice CF, Carmody RN, *et al*. Diet rapidly and reproducibly alters the human gut microbiome. *Nature* 2014;505:559–63.
13 Wang M, Liu X, Chang G, *et al*. Single-Cell RNA sequencing analysis reveals sequential cell fate transition during human spermatogenesis. *Cell Stem Cell* 2018;23:599–614.
14 Sohni A, Tan K, Song H-W, *et al*. The neonatal and adult human testis defined at the single-cell level. *Cell Rep* 2019;26:1501–17.
15 Hermann BP, Cheng K, Singh A, *et al*. The mammalian spermatogenesis single-cell transcriptome, from spermatogonial stem cells to spermatids. *Cell Rep* 2018;25:1650–67.
16 Martin F-PJ, Dumas M-E, Wang Y, *et al*. A top-down systems biology view of microbiome-mammalian metabolic interactions in a mouse model. *Mol Syst Biol* 2007;3:112.
17 Claus SP, Tsang TM, Wang Y, *et al*. Systemic multicompartmental effects of the gut microbiome on mouse metabolic phenotypes. *Mol Syst Biol* 2008;4:219.
18 Buaas FW, Kirsh AL, Sharma M, *et al*. Plzf is required in adult male germ cells for stem cell self-renewal. *Nat Genet* 2004;36:647–52.
19 White JC, Highland M, Kaiser M, *et al*. Vitamin A deficiency results in the dose-dependent acquisition of anterior character and shortening of the caudal hindbrain of the rat embryo. *Dev Biol* 2000;220:263–84.
20 Kaiser ME, Merrill RA, Stein AC, *et al*. Vitamin A deficiency in the late gastrula stage rat embryo results in a one to two vertebral anteriorization that extends throughout the axial skeleton. *Dev Biol* 2003;257:14–29.
21 van Pelt AM, de Rooij DG. Retinoic acid is able to reinitiate spermatogenesis in vitamin A-deficient rats and high replicate doses support the full development of spermatogenic cells. *Endocrinology* 1991;128:697–704.
22 Vernet N, Dennefeld C, Rochette-Egly C, *et al*. Retinoic acid metabolism and signaling pathways in the adult and developing mouse testis. *Endocrinology* 2006;147:96–110.
23 Koubova J, Menke DB, Zhou Q, *et al*. Retinoic acid regulates sex-specific timing of meiotic initiation in mice. *Proc Natl Acad Sci U S A* 2006;103:2474–9.
24 Bowles J, Knight D, Smith C, *et al*. Retinoid signaling determines germ cell fate in mice. *Science* 2006;312:596–600.
25 Bowles J, Koopman P. Retinoic acid, meiosis and germ cell fate in mammals. *Development* 2007;134:3401–11.
26 Snyder EM, Small C, Griswold MD. Retinoic acid availability drives the asynchronous initiation of spermatogonial differentiation in the mouse. *Biol Reprod* 2010;83:783–90.
27 Griswold MD, Hogarth CA, Bowles J, *et al*. Initiating meiosis: the case for retinoic acid. *Biol Reprod* 2012;86:35.
28 Sandell LL, Sanderson BW, Moiseyev G, *et al*. Rdh10 is essential for synthesis of embryonic retinoic acid and is required for limb, craniofacial, and organ development. *Genes Dev* 2007;21:1113–24.
29 Sandell LL, Lynn ML, Inman KE, *et al*. Rdh10 oxidation of vitamin A is a critical control step in synthesis of retinoic acid during mouse embryogenesis. *PLoS One* 2012;7:e30698.
30 Niederreither K, Dollé P. Retinoic acid in development: towards an integrated view. *Nat Rev Genet* 2008;9:541–53.
31 Chung SSW, Wolgemuth DJ. Role of retinoid signaling in the regulation of spermatogenesis. *Cytogenet Genome Res* 2004;105:189–202.
32 Alfano M, Pederzoli F, Locatelli I, *et al*. Impaired testicular signaling of vitamin A and vitamin K contributes to the aberrant composition of the extracellular matrix in idiopathic germ cell aplasia. *Fertil Steril* 2019;111:687–98.
33 Beydoun MA, Shroff MR, Chen X, *et al*. Serum antioxidant status is associated with metabolic syndrome among U.S. adults in recent national surveys. *J Nutr* 2011;141:903–13.
34 Trasino SE, Benoit YD, Gudas LJ. Vitamin A deficiency causes hyperglycemia and loss of pancreatic β-cell mass. *J Biol Chem* 2015;290:1456–73.
35 Higuchi K, Saito I, Maruyama K, *et al*. Associations of serum β-carotene and retinol concentrations with insulin resistance: the Toon health study. *Nutrition* 2015;31:975–80.
36 Brun P-J, Grijalva A, Rausch R, *et al*. Retinoic acid receptor signaling is required to maintain glucose-stimulated insulin secretion and β-cell mass. *Faseb J* 2015;29:671–83.
37 Trasino SE, Benoit YD, Gudas LJ. Vitamin A deficiency causes hyperglycemia and loss of pancreatic β-cell mass. *J Biol Chem* 2015;290:1456–73.
38 Eroglu A, Harrison EH. Carotenoid metabolism in mammals, including man: formation, occurrence, and function of apocarotenoids. *J Lipid Res* 2013;54:1719–30.

Supplemental Information for

Disrupted spermatogenesis in a metabolic syndrome model: the role of vitamin A metabolism in the gut-testis axis

This file includes:

Materials and Methods

Supplementary figures 1 to 12 and figure legends

Supplementary tables 1 to 3

Materials and Methods

Animal models. All animal procedures were approved and conducted in accordance with the Inner Mongolia University Animal Care and Use Committee. ICR mice were obtained from Inner Mongolia University. Mice were kept at a constant temperature of 22 ± 2°C on a 12 h light/dark cycle and had unrestricted access to food and water. Mongolia male sheep experiments were accomplished at the Inner Mongolia University Experimental Station. Before the experiment, they were acclimatized to the environment with free access to food and water for at least 1 week. Sheep were randomly distributed and fed with a standard chow diet (ND) or a medium-energy (MED) or a high-energy diet (HED) (supplementary tables 1 and 2). The amount of essential vitamin supplementation was nearly the same.

Morphology and immunofluorescence. Testis tissues were quickly collected, fixed in 4% paraformaldehyde, placed in 70% ethanol, dehydrated and embedded in paraffin. The testis were serially sectioned into 5 μm sections. After deparaffinization (at 60 °C for 2 hours), the sections were prepared and stained with hematoxylin and eosin. Within the group, five testicular cross-sections which were at least 50 sections apart from each animal were examined.

For immunofluorescence, the sections were performed in 0.01 mol/L sodium citrate at 95 °C for 10 minutes. Samples were then blocked with BDT (3% BSA, 10% normal donkey serum in TBS) for 30 minutes. Antibody source and dilutions were as follows: MVH (abcam, ab27591, 1:200), STRA8 (abcam, ab49602, 1:300), SYCP3 (abcam, ab15093, 1:300), RDH10 (proteintech, 14644-1-AP, 1:200), RBP4

(proteintech, 11774-1-AP, 1:200), PLZF (abcam, ab189849, 1:200). Sections were examined under a Nikon fluorescence microscope (A1, Japan).

Single cell library preparation, sequencing and analysis. Single cell libraries were prepared using the 10×Genomics Chromium Single Cell 3′Library & Gel Bead Kit v2 (10×Genomics Inc, USA) following the manufacturer's instructions. Briefly, we obtained testicular cells from freshly isolated testicular samples. Testes were minced with sterilized scissors after washing three times with PBS. Mixed testes samples from each group were collected and digested in collagenase type IV (1 mg/ml) at 37°C for 15 min. The digestion process was stopped with DMEM (containing 10% FBS). The cell suspension was filtered with a 40μm cell strainer (BD Biosciences, USA). After centrifugation, the cells were suspended three times in PBS solution supplemented with 0.04% BSA (Sigma, USA).

The cell viability and cell concentration were evaluated before cDNA library construction. Trypan blue staining with a haemocytometer (Bio-Rad, USA) was applied to detect the cell viability (>80%). Then the concentration was 1000 cells/μl for loading to the single cell chip. Chromium 10×Single Cell System (10×Genomics, USA) was applied to form the Gel-Bead in Emulsions (GEMs) system. Then cells were barcoded and cDNA library was constructed. The sequencing was done by an Illumina NovaSeq 6000 (Illumina, USA) with pair end 150 bp (PE150) reads.

The raw sequencing data was processed using CellRanger v3.0.2 software according to 10×Genomics official pipeline (https://www.10xgenomics.com/). The 10×Genomics pre-built sheep genome for Oar_rambouillet_v1.0 was referenced. Then, the cell clustering and quality control were analyzed with scRNA-seq Seurat software (v3.1.5). After characterization of all cell clusters in testes samples, cells were further clustered based on their cell identity. After clustering, cluster-specific marker genes were identified using the "FindAllMarkers" function. The UMAP identified cell clusters were annotated with based on the previously reported canonical marker genes expression. Differential expression genes were used for enrichment analysis in Metascape (http://metascape.org). To interpret cell differentiation fate decisions, Monocle 2 (v2.16.0) was used to determine the single-cell pseudo-time trajectory according to the official tutorial (http://cole-trapnell-lab.github.io/monocle-release/docs/#constructing-single-cell-trajectories). To perform pseudo-time ordering to particular cell types, we firstly subclustered interested cell type from Seurat object.

Then, the Monocle object was constructed using the Monocle implemented "newCellDataSet" function from the Seurat object.

Metabolomics profiling of small intestine digesta samples. Small intestine digesta samples were collected and immediately stored at liquid nitrogen. 25 mg of samples was homogenized with 500 μL extract solution (acetonitrile: methanol: water = 2: 2: 1). The samples were homogenized at 35 Hz for 4 min and sonicated for 5 min in ice-water bath. All samples were incubated at -40°C for 1h and centrifuged at 12000 rpm for 15 min at 4°C. Then supernatant was transferred to a fresh tube and dried in a vacuum concentrator at 37°C. The dried samples were reconstituted in 200 μL of 50% acetonitrile by sonication on ice for 10 min. The samples were subsequently centrifuged at 13,000 rpm for 15 min at 4°C. The supernatants were subjected to metabolomics profiling by UHPLC-QTOF-MS.

Liquid chromatographic separation for processed small intestine digesta samples was achieved on a UPLC BEH Amide column (100 mm × 2.1 mm, 1.7 μm, Waters) using a 1290 Infinity series UHPLC System (Agilent Technologies). The mobile phase was composed of 25 mM ammonium acetate and 25 mM ammonia hydroxide in water (A) and acetonitrile (B). The flow rate was set at 0.5 ml/min with the following optimal gradient elution condition: 0 to 0.5 min, 95% B; 0.5 to 7.0 min, 95%~65% B; 7.0 to 8.0 min, 65%~40% B; 8.0 to 9.0 min, 40% B; 9.0 to 9.1 min, 40%~95% B; 9.1 to 12.0 min, 95% B. The column temperature was 25°C. The auto-sampler temperature was 4°C. The injection volume was 2 μl (pos) or 2 μl (neg), respectively.

For LC/MS experiment, the TripleTOF 6600 mass spectrometry was used for its ability to acquire MS/MS spectra on an information-dependent bass (IDA). The cycle time was set at 0.56s. In each cycle, the most intensive 12 precursor ions with intensity above 100 were chosen for MS/MS at collision energy of 30 eV. The operation conditions were set as following: Gas 1, 60 psi; Gas 2, 60 psi; Curtain Gas, 35 psi; Source Temperature, 600°C; Declustering potential, 60 V; Ion Spray Voltage Floating, 5000 V (pos) or -4000 V (neg), respectively. In this mode, data were monitored by acquisition software (Analyst TF 1.7, AB Sciex). MS raw data files were converted to the mzXML format by ProteoWizard, and processed by R package XCMS (version 3.2).

16S rDNA amplicon sequencing and bioinformatics analysis. Genomic DNA of small intestine digesta samples was extracted using a QIAGEN kit, and quantified using a Qubit 2.0 fluorometer (Invitrogen, USA). The V3, V4 hypervariable regions of the 16S rDNA gene was selected for generating amplicons using universal primers with barcode. DNA libraries were recovered using a GeneJET Gel Extraction Kit (Thermo Scientific, USA), and quantified using a Qubit 2.0 fluorometer. The purified DNA libraries were constructed with NEB NextR UltraTM DNA Library Prep Kit for Illumina according to the manufacturer's instructions and index codes were added (NEB, United States). Then, the DNA libraries were sequenced using the 250 bp paired-end strategy on the Illumina platform according to the standard protocol (Illumina, USA). To get the raw tags, paired-end reads were merged by FLASH (V1.2.7). Then raw tags were filtered and clustered by FASTX-Toolkit. We identified possible chimeras by employing UCHIME. The denoised sequences were clustered using USEARCH (version 10.0) and tags with similarity≥97% were regarded as an operational taxonomic units (OTUs) using MOTHUR pipeline. Taxonomy was assigned to all OTUs by searching against the Silva databases using the uclust within QIIME. The Principal coordinate analysis (PCoA), taxonomy, and heatmap of differential abundance were calculated and visualized using R software.

Sperm smear and sperm count measurement. The cauda epididymis was dissected from adult sheep, and incubated for 30 min at 37℃ to release spermatozoa. Spermatozoa were suspended in 1 ml phosphate-buffered saline, washed three times, spread onto slides, and fixed for staining. The viewing areas were captured using a CCD camera. The sperm count was quantified by using a haemocytometer under a Nikon light microscope.

PCR and Real-time quantitative PCR (qPCR) analyses. Genomic DNA of small intestine digesta samples and fecal were extracted using a EasyPure® Stool Genomic DNA Kit, and quantified using a Qubit 2.0 fluorometer (Invitrogen, USA). The primer for *Ruminococcaceae_NK4A214_group* (forward:5'-AACTCATAAACTGCATTTGAAACTGTACT-3' and reverse: 5'-AGCGTCAGTTGCTGTCCAGTAGAC-3') and total bacterium (forward:5'-ACTCCTACGGGAGGCAGCAG-3' and reverse: 5'-ATTACCGCGGCTGCTGG-3') were used. Real-time PCR was carried out with the Roche Light Cycler 480II System.

Western blot analysis. For western blot analyses, testis were extracted in cold RIPA buffer on ice, which supplemented with 1 mM phenylmethylsulfonyl fluoride and a protease inhibitor cocktail (Roche, USA). The protein lysates were collected and resolved by SDS-PAGE, then transferred onto a polyvinylidene fluoride membrane (Millipore, IPVH00010, Germany) and probed with the primary antibodies. Antibodies were diluted as follows: STRA8 (abcam, ab49602, 1:1000), RDH10 (proteintech, 14644-1-AP, 1:1000), PLZF (abcam, ab189849, 1:1000), GAPDH (proteintech, 60004-1-IG, 1:5000), β-ACTIN (sigma, A1978, 1:10000).

Targeted vitamin A and total bile acid quantification. Vitamin A was quantified by a UPLC I Class system (Agilent 1290 infinity UHPLC) on a C-18 column (Waters, BEH C18 1.7μm, 2.1 mm×50 mm column). Testes samples (100mg) were transferred to a clean centrifuge tube after being thawed on ice. Internal standard solution (10μL), water-acetonitrile-methanol (1:2:2, v/v/v, 0.5 mL) and several 1.0 mm ceramic beads were added, and then homogenized using Biospec MiniBeadbeater before centrifuged at 14,000g for 10min at 4°C. Then, the supernatant was analyzed using HPLC-MS/MS. Mass spectrometry analysis was performed using 5500 QTRAP (AB SCIEX). The 5500 QTRAP APCI source conditions were as follows: source temperature: 550°C; Gas1: 55; Gas2: 55; Curtain gas: 40; IonSapary Voltage Floating: +5500V. MRM method was used for MS quantitative data acquisition.

For serum and testicular vitamin A measurements, serum and testes samples were processed for vitamin A concentration assays by a ELISA kit (Novus, NBP2-60192). For retinene measurements, transplanted material samples were processed for retinene concentration assays by a kit (Dogesce, DG96139Q). For total bile acid measurements, transplanted material samples were processed for TBA concentration assays by a kit (Nanjing Jiancheng Bioengineering Institute, E003-2-1).

Blood glucose examination during Glucose Tolerance Tests (GTT) and Insulin Tolerance Tests (ITT). During GTT, an intravenous injection of glucose with a single dose of 2g/kg body weight was performed in 12h-fasted sheep. Blood samples were collected before glucose injection (0 min) and at 30, 60, 90, 120 and 160 min afterward. During ITT, an intravenous injection of insulin with a single dose of 0.75

IU/kg body weight was performed in 12h-fasted sheep. Blood samples were collected before insulin injection (0 min) and at 30, 60, 90 and 120 min afterward. Blood glucose concentration were immediately measured by gas chromatograph-mass spectrometer (GCMS-QP2010ultra).

Fecal microbiota transplantation. The small intestine luminal content (microbiota) from each group was collected from donor sheep and pooled. The 1g fecal samples were diluted with 1ml 20% sterile glycerol (saline), homogenized and frozen. Before inoculation, fecal samples were diluted in sterile saline to a working concentration of 0.05 g/ml and filtered through a 70-μm cell strainer. Fresh transplanted material was prepared within 10 min before oral gavage to prevent changes in bacterial composition. Three-week-old male ICR mice were used in current investigation. The recipient mice were treated with fresh transplant material from either ND-treated sheep or HED-treated sheep. Oral gavage with fecal transplant material was conducted daily through the 8-week experiment.

Statistics. GraphPad Prism（USA） was used for statistical analysis. The results of biological assay are presented as means ± SEM. All results were considered statistically significant at $P < 0.05$. Statistical significance between two groups was determined by Student's t test. One-way analysis of variance (ANOVA) followed by Tukey's multiple comparison's test was used to assess the statistical significance of differences among three or more groups. Differential metabolites were defined as those with variable importance in the projection (VIP) >1.0 and adjusted *P* values less than 0.05.

Supplementary figures and figure legends

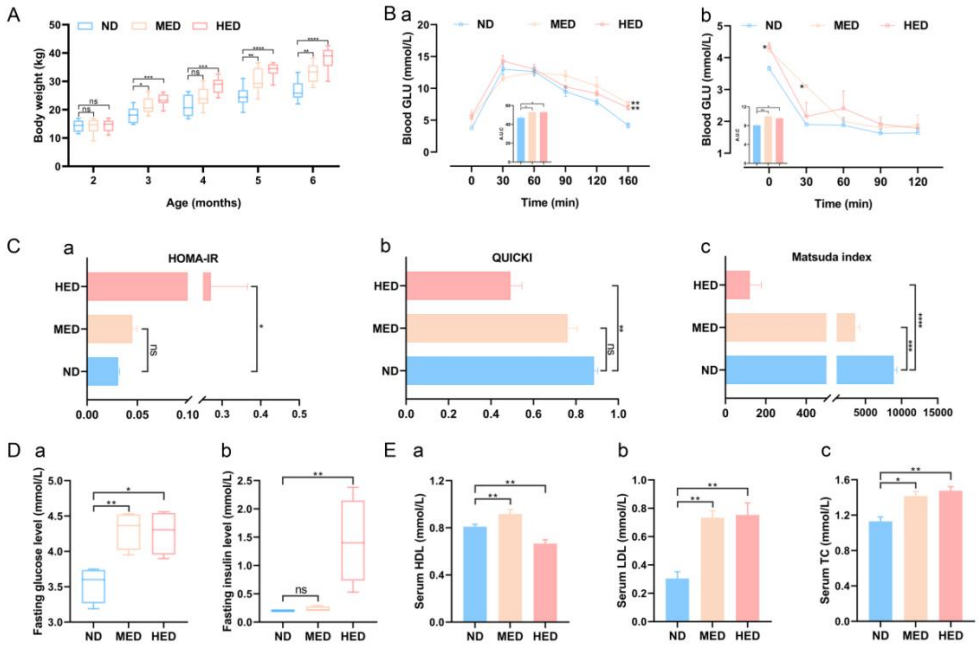

Supplementary figure 1 Consumption of an excessive-energy diet caused symptoms of metabolic disorder in the sheep model. Sheep were randomly divided into three groups, which involved continuous feeding with a long-term high-calorie diet for six months beginning at two months of age. The experiment included three treatments: a normal diet (ND), a medium-energy diet (MED), and a high-energy diet (HED). (A) Body weights of the ND, MED, and HED-fed groups over a period of 6 months. (B) (a) Glucose tolerance test (GTT) and (b) insulin tolerance test (ITT) with area under the curve (AUC) in the ND, MED, and HED groups. (C) (a) HOMA-IR, (b) QUICKI, and (c) Matsuda indexes were calculated for the three groups. (D) Fasting (a) glucose and (b) insulin levels in the three groups. (E) (a) HDL, (b) LDL, and (c) total TC levels in blood serum from the three groups. **P* <0.05, ***P* <0.01, ****P* <0.001, *****P* <0.0001. ns, no significant difference.

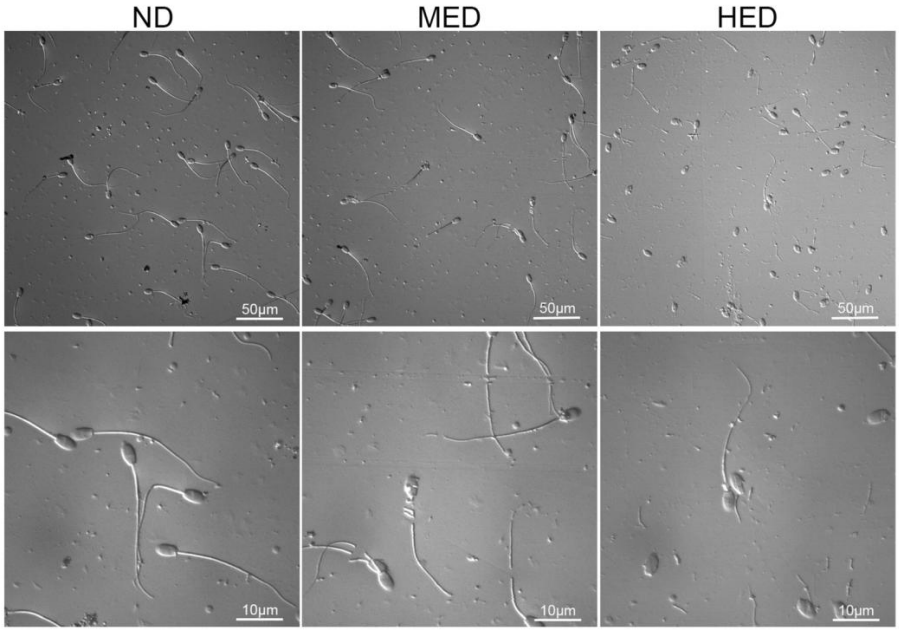

Supplementary figure 2 Morphology of the spermatozoa from ND, MED, and HED groups. The representative sperm smear for morphology with multiple magnifications. Scale bar = 50 μm and 10 μm.

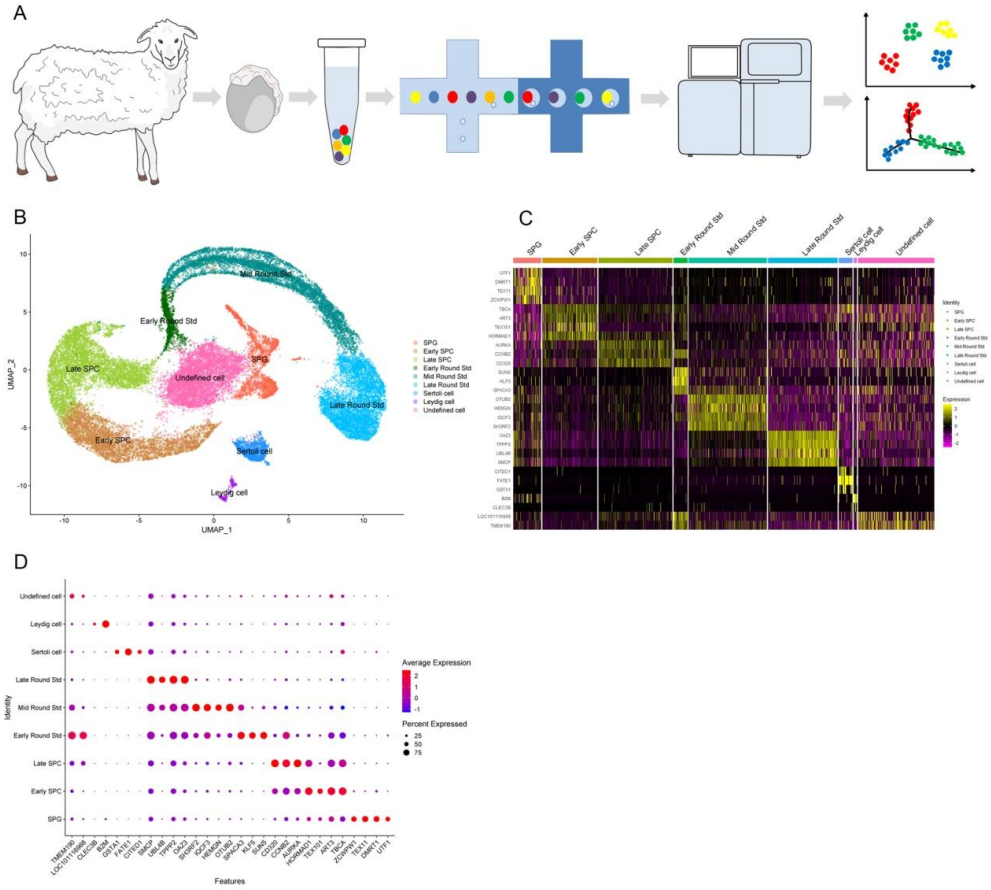

234

235 **Supplementary figure 3 10X Genomics profiling of sheep spermatogenic cells.** (A)
236 Schematic diagram of the scRNA-seq analysis procedure. (B) UMAP plot of testes
237 clusters defined by scRNA-seq analysis. (C) Heatmap of the most common
238 differentially expressed genes (DEGs) from nine clusters. (D) Dot plot of marker
239 genes expressed in the nine clusters.

240

241

242

243

244

245

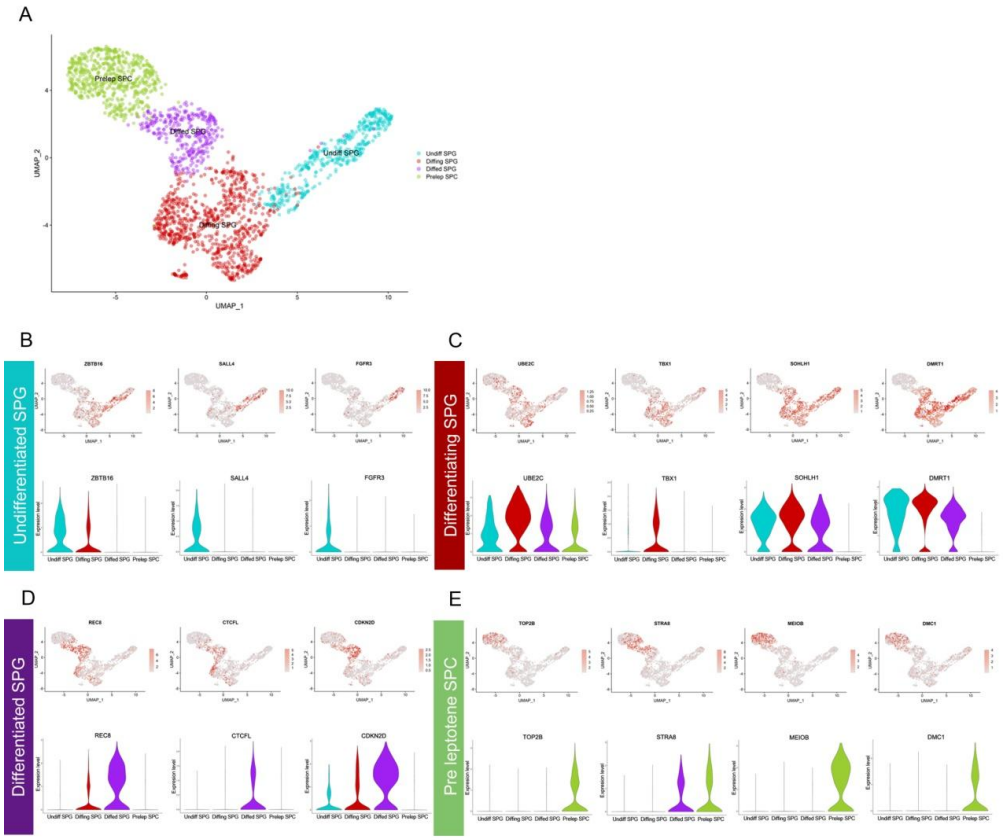

Supplementary figure 4 Identification and characterization of sheep SPG subsets. (A) UMAP plot of SPG subsets. (B-E) UMAP plot, violin plot of undifferentiated SPG (undiffed SPG), differentiating SPG (diffing SPG), differentiated SPG (diffed SPG), and pre-leptotene SPC (pre-L-SPC) marker genes.

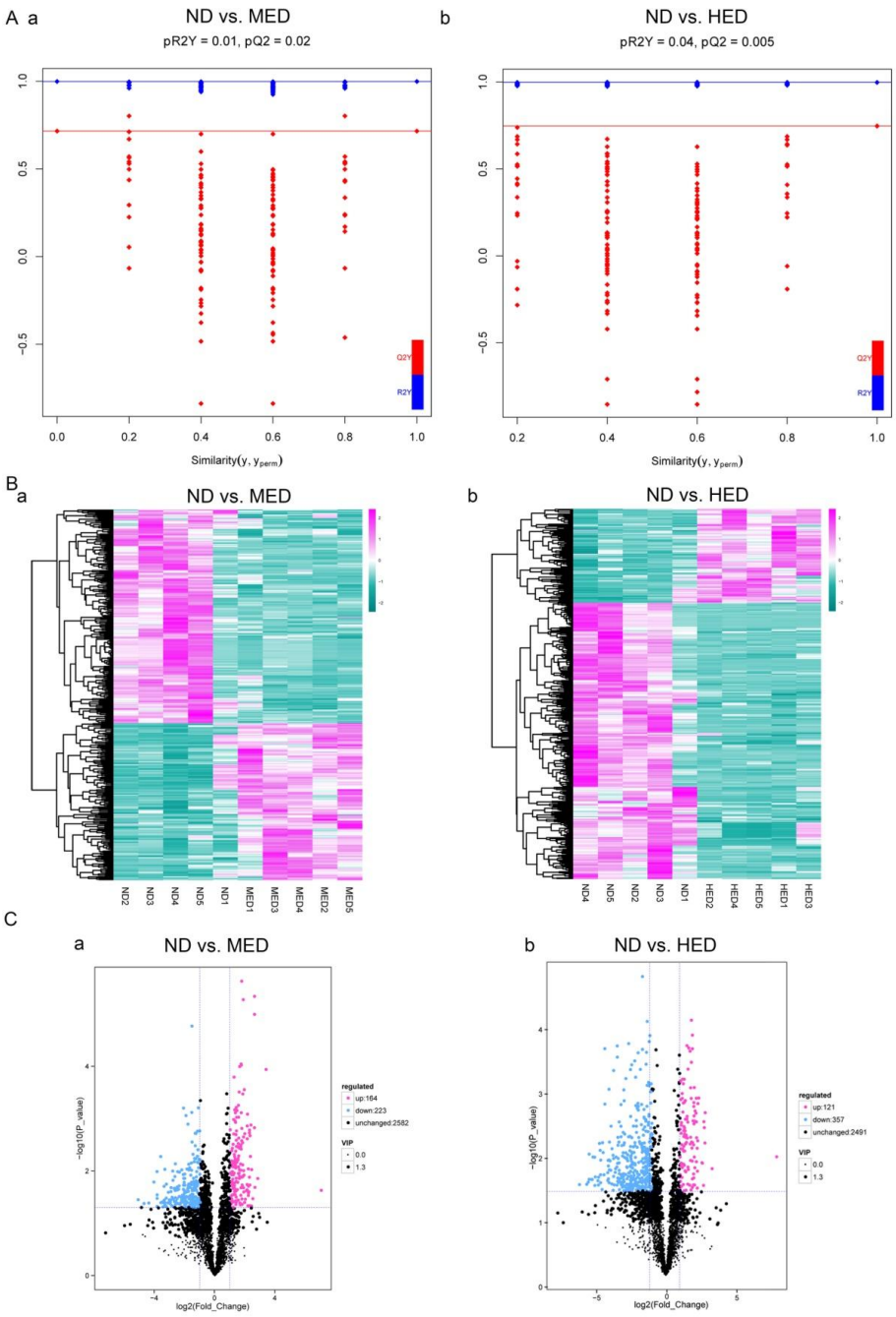

Supplementary figure 5 Metabolomics profiling was altered in a MetS model. (A) PLS-DA validation diagram in (a) ND vs. MED comparison and (b) ND vs. HED comparison. (B) Heatmaps of general differential metabolites in (a) ND vs. MED comparison and (b) ND vs. HED comparison. (C) Volcano plots of general differential metabolites in (a) ND vs. MED comparison and (b) ND vs. HED comparison.

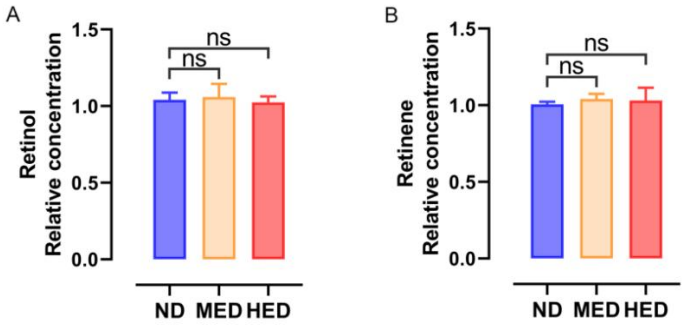

Supplementary figure 6 Concentration analysis of retinol and retinene in the diet from ND, MED and HED groups. Analysis of (A) retinol and (B) retinene levels in each indicated group. ns, no significant difference.

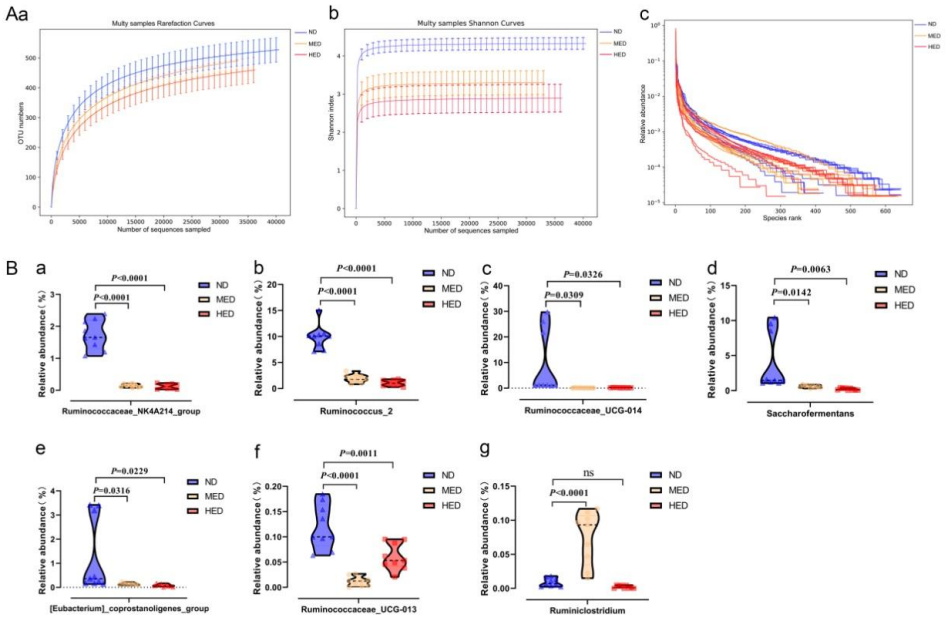

282

283 **Supplementary figure 7 The α-diversity of gut microbiota and the abundance of**
284 **genus-level gut microbiota belonging to *Ruminococcaceae* in a MetS model.** (A)
285 (a) rarefaction curves, (b) Shannon curves, and (c) OTU rank curves of gut microbiota
286 for ND, MED, and HED samples. (B) Comparison of the relative abundance of genus-
287 level bacteria (a) *Ruminococcaceae_NK4A214_group*, (b) *Ruminococcus_2*, (c)
288 *Ruminococcaceae_UCG-014*, (d) *Saccharofermentans*, (e)
289 *[Eubacterium]_coprostanoligenes_group,* (f) *Ruminococcaceae_UCG-013*, (g)
290 *Ruminiclostridium* belonging to *Firmicutes Ruminococcaceae* in the indicated groups.
291 ns, no significant difference.
292

293

294

295

296

297

298

299

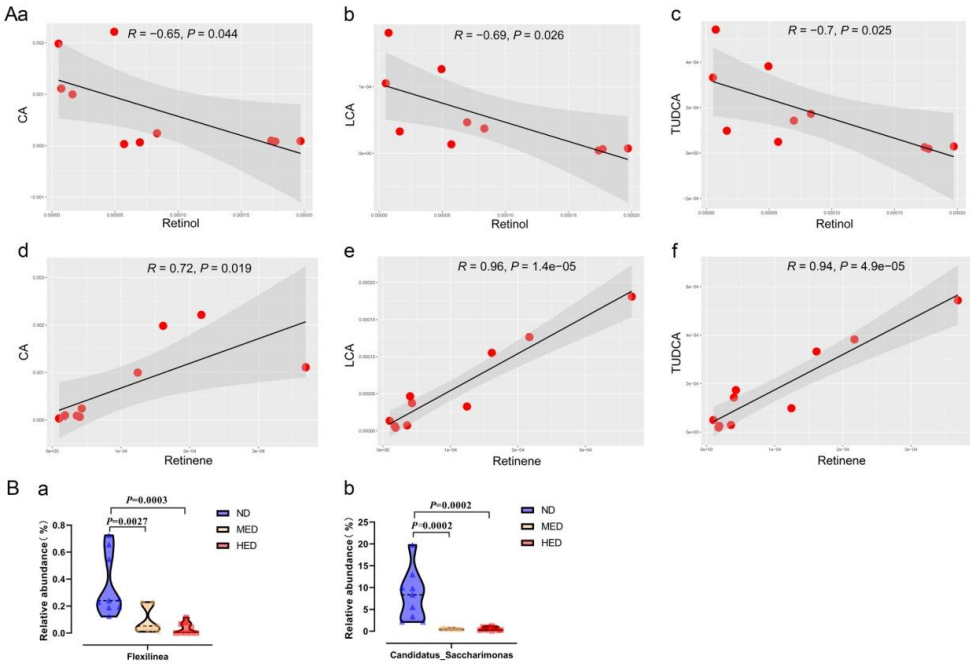

Supplementary figure 8 Correlation analysis of differential metabolites and related genus-level gut microbiota was altered in a MetS model. (A) Pearson's correlation analysis of (a-c) retinol, (d-f) retinene levels with cholic acid (CA), lithocholic acid (LCA), and tauroursodeoxycholic acid (TUDCA) levels. (B) Comparison of the relative abundance of (a) *Flexilinea*, (b) *Candidatus_Saccharimonas* in the indicated groups.

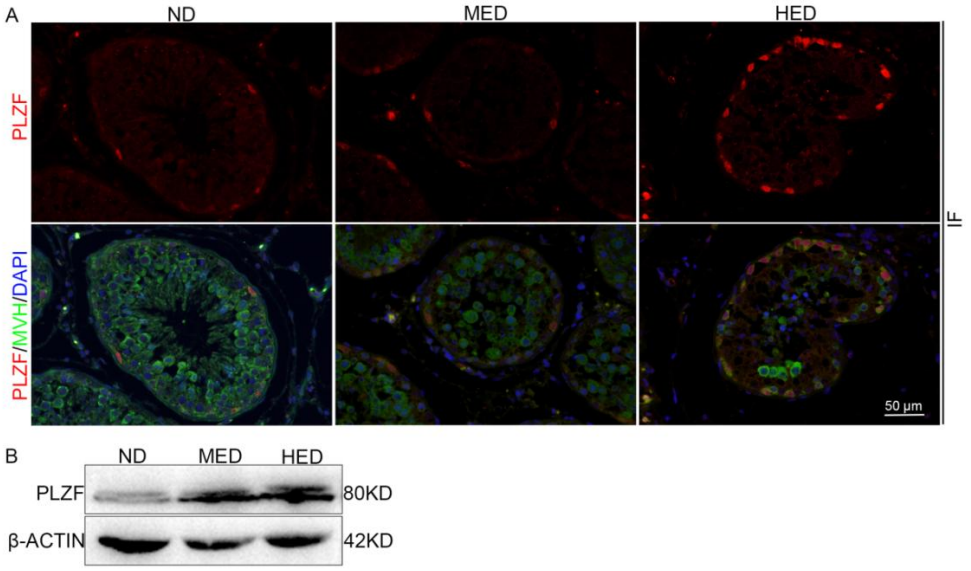

Supplementary figure 9 The expression analysis of undifferentiated spermatogonia marker gene PLZF. (A) The representative images of PLZF immunofluorescence (IF) staining in sections of testicular tissue. Scale bar = 50 μm. (B) Western blotting of PLZF and β-ACTIN in each indicated group.

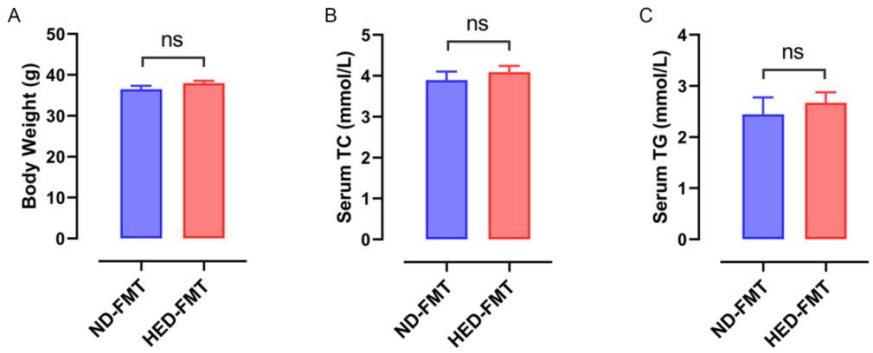

Supplementary figure 10 Analysis of body weight, serum TC levels, and serum TG levels between ND-FMT and HED-FMT groups. Analysis of (A) body weight, (B) serum TC levels, and (C) serum TG levels in each indicated group. ns, no significant difference.

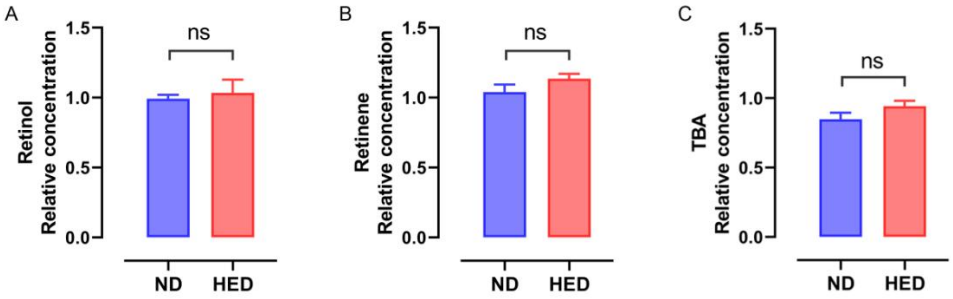

Supplementary figure 11 Analysis of transmitted material from the donors ND and HED groups. (A) Analysis of retinol levels in each indicated group. (B) Analysis of retinene levels in each indicated group. (C) Analysis of total bile acid (TBA) levels in each indicated group. ns, no significant difference.

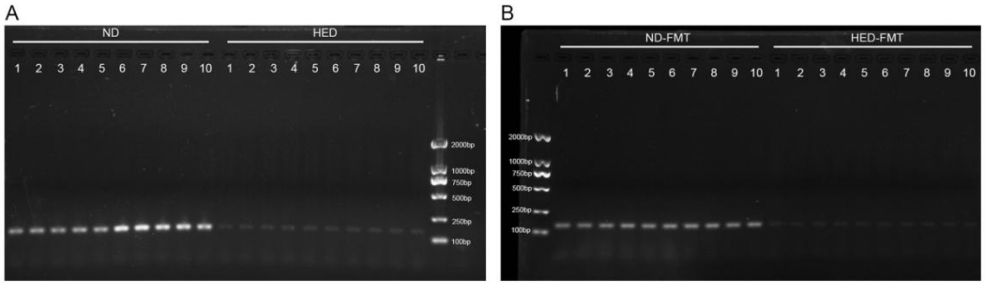

Supplementary figure 12 Comparison of the relative abundance of *Ruminococcaceae_NK4A214_group*. (A) The PCR analysis of *Ruminococcaceae_NK4A214_group* abundance in the transmitted material from the donors ND and HED groups. (B) The PCR analysis of *Ruminococcaceae_NK4A214_group* abundance in faecal samples from ND-FMT and HED-FMT groups.

Supplementary table 1 Effective energy per kg of diet (Unit: Mcal)

Groups	ND	MED	HED
Effective Energy	1.05	1.46	2.01

Supplementary table 2 The percentage of nutrient composition

Nutrients/Groups	ND (%)	MED (%)	HED (%)
Protein	16.61	20.99	25.31
Fat	3.24	3.54	3.83
Carbohydrates	80.15	75.47	70.86

Supplementary table 3 The rate of cell viability and cell aggregation

Groups	Cell Viability (%)	Cell Aggregation Ratio (%)
ND	88.00	4.84
MED	87.50	2.77
HED	89.42	1.89